

Coupled-channel effects in ω photoproduction near threshold

Yongseok Oh*

*Institute of Physics and Applied Physics,
Department of Physics, Yonsei University, Seoul 120-749, Korea*

T.-S. H. Lee†

Physics Division, Argonne National Laboratory, Argonne, Illinois 60439

Abstract

The coupled-channel effects on ω photoproduction near threshold have been investigated in a model that all relevant transition amplitudes are calculated from the tree diagrams of effective Lagrangians. With the parameters constrained by the data of $\gamma N \rightarrow \pi N$, $\gamma N \rightarrow \rho N$, and $\pi N \rightarrow \omega N$ reactions, it is found that the coupled-channel effects due to the intermediate πN and ρN states can significantly change the differential cross sections and spin observables. Our results suggest strongly that the coupled-channel effects should be taken into account in extracting reliable resonance parameters from the data of vector meson photoproduction in the resonance region.

PACS numbers: 13.60.Le, 13.75.Gx, 13.88.+e, 25.20.Lj

*Electronic address: yoh@phya.yonsei.ac.kr

†Electronic address: lee@theory.phy.anl.gov

I. INTRODUCTION

Experimental data of vector meson photoproductions are now being rapidly accumulated at Bonn [1], Thomas Jefferson National Accelerator Facility [2], GRAAL of Grenoble [3], and LEPS of SPring-8 [4]. The study of photoproduction of vector mesons (ω, ρ, ϕ) is expected to be useful to resolve the so-called “missing resonances” problem [5]. In addition, the extracted resonance parameters can shed lights on the structure of nucleon resonances (N^*) and can be used to test the existing hadron models. In recent years, some theoretical progress has been made [6, 7] in this direction. In this work we will address the question about how these earlier models should be improved for a more reliable extraction of the N^* parameters from the forthcoming data. To be specific, we consider the photoproduction of ω meson.

It is well known that the extraction of N^* parameters from experimental data depends strongly on the accuracy of our treatment of the non-resonant amplitudes. In all of the recent studies of ω photoproduction at resonance region [6, 7], the non-resonant amplitudes are calculated from the tree diagrams of effective Lagrangians. This is obviously not satisfactory for the following reasons. First, the tree-diagram models are not unitary. The importance of the unitary condition in interpreting the data has been demonstrated in the study of pion photoproductions. For example, the calculations of Ref. [8] have shown that the magnetic $M1$ amplitude of the $\gamma N \rightarrow \Delta(1232)$ transition can be identified with the predictions from constituent quark models only when the pion re-scattering effects (i.e., pion cloud effects), as required by the unitary condition, are accounted for appropriately in analyzing the data. Second, the vector meson productions occur in the energy region where several meson-nucleon channels are open and their influence must be accounted for. This coupled-channel effect was already noticed and explored in 1970’s for vector meson photoproduction [9]. In this paper we make a first attempt to re-investigate this problem in conjunction with the approach developed in Ref. [7].

This paper is organized as follows. In Sec. II, we introduce a unitary coupled-channel formulation of γN reaction and indicate the procedures we will use to investigate ω photoproduction. Section III is devoted to specify various transition amplitudes which will be used as the inputs to our calculations. Numerical results are presented and discussed in Sec. IV. Possible future development are outlined in Sec. V. Some details on the $\pi N \rightarrow \omega N$ reaction are given in Appendix.

II. DYNAMICAL COUPLED-CHANNEL FORMULATION

In the considered energy region, the γN reaction is a multi-channel multi-resonance problem. In this work we follow the dynamical approach developed by Sato and Lee [8] to investigate this problem. It is done by simply extending the scattering formulation of Ref. [8] to include more N^* states and more meson-nucleon channels. The resulting amplitude $T_{\gamma N, \omega N}(E)$ for the $\gamma N \rightarrow \omega N$ reaction can be written as

$$T_{\gamma N, \omega N}(E) = t_{\gamma N, \omega N}(E) + \sum_{N^*} \frac{\bar{\Gamma}_{\gamma N \rightarrow N^*} \bar{\Gamma}_{N^* \rightarrow \omega N}}{E - M_{N^*}^0 - \Sigma_{N^*}(E)}, \quad (1)$$

where $t_{\gamma N, \omega N}$ is the non-resonant amplitude. It is defined by the following coupled-channel equations

$$t_{\gamma N, \omega N} = B_{\gamma N, \omega N} + \sum_{\alpha} B_{\gamma N, \alpha} G_{\alpha}(E) t_{\alpha, \omega N}, \quad (2)$$

$$t_{\alpha,\beta} = v_{\alpha,\beta} + \sum_{\delta} v_{\alpha,\delta} G_{\delta}(E) t_{\delta,\beta}, \quad (3)$$

where α, β denote the considered meson-nucleon channels such as ωN , πN , and ρN . $B_{\gamma N, \alpha}$ is the non-resonant photoproduction amplitude, $v_{\alpha,\beta}$ are the non-resonant meson-nucleon interactions, and G_{α} is the free meson-nucleon propagator defined by

$$G_{\alpha}(E) = \frac{1}{E - (H_0)_{\alpha} + i\epsilon}. \quad (4)$$

The N^* excitations are described by the second term of Eq. (1). It is defined by the dressed vertex functions

$$\begin{aligned} \bar{\Gamma}_{\gamma N \rightarrow N^*} &= \Gamma_{\gamma N \rightarrow N^*} + \sum_{\alpha} v_{\gamma N, \alpha} G_{\alpha}(E) \bar{\Gamma}_{\alpha \rightarrow N^*}, \\ \bar{\Gamma}_{N^* \rightarrow \omega N} &= \Gamma_{N^* \rightarrow \omega N} + \sum_{\alpha} \Gamma_{N^* \rightarrow \alpha} G_{\alpha}(E) t_{\alpha, \omega N}, \end{aligned} \quad (5)$$

and the N^* self-energy

$$\Sigma_{N^*}(E) = \sum_{\alpha} \bar{\Gamma}_{N^* \rightarrow \alpha} G_{\alpha}(E) \Gamma_{\alpha \rightarrow N^*}. \quad (6)$$

The bare mass $M_{N^*}^0$ of Eq. (1) and the bare vertices $\Gamma_{\gamma N \leftrightarrow N^*}$ and $\Gamma_{\alpha \leftrightarrow N^*}$ of Eq. (5) can be identified with the predictions from a hadron model that does not include the continuum meson-baryon states.

In this paper, we focus on the calculation of the non-resonant amplitudes defined by Eq. (2). The extraction of resonance parameters from the data depends heavily on the accuracy of this dynamical input. Because of the limitation of the strong interaction data, we will only consider the coupled-channel effects due to the πN and ρN channels. To further simplify the calculations, we will assume that the meson-nucleon scattering amplitudes in Eq. (3) can be calculated from the tree-diagrams of effective Lagrangians, but with their parameters constrained by the available data. This is certainly not very satisfactory, but it should be sufficient for this exploratory investigation.

III. NON-RESONANT AMPLITUDES

We assume that all the non-resonant amplitudes in Eqs. (2) and (3) can be calculated from the tree-diagrams defined by the following effective Lagrangian,

$$\mathcal{L} = \mathcal{L}_{V\gamma\varphi} + \mathcal{L}_{VV\varphi} + \mathcal{L}_{\varphi NN} + \mathcal{L}_{\sigma} + \mathcal{L}_{\gamma NN} + \mathcal{L}_{VNN}, \quad (7)$$

where

$$\begin{aligned} \mathcal{L}_{V\gamma\varphi} &= \frac{eg_{\rho\gamma\pi}}{2M_{\rho}} \varepsilon^{\mu\nu\alpha\beta} \text{Tr} [\partial_{\mu}\rho_{\nu}\partial_{\alpha}A_{\beta}\pi] + \frac{eg_{\omega\gamma\pi}}{2M_{\omega}} \varepsilon^{\mu\nu\alpha\beta} \text{Tr} [\partial_{\mu}\omega_{\nu}\partial_{\alpha}A_{\beta}\pi\tau^3] \\ &\quad + \frac{eg_{\omega\gamma\eta}}{M_{\omega}} \varepsilon^{\mu\nu\alpha\beta} \partial_{\mu}\omega_{\nu}\partial_{\alpha}A_{\beta}\eta, \\ \mathcal{L}_{VV\varphi} &= \frac{g_{\omega\rho\pi}}{2} \varepsilon^{\mu\nu\alpha\beta} \text{Tr} [\partial_{\mu}\omega_{\nu}\partial_{\alpha}\rho_{\beta}\pi], \end{aligned}$$

$$\begin{aligned}
\mathcal{L}_{\varphi NN} &= \frac{g_{\pi NN}}{2M_N} \bar{\psi} \gamma^\mu \gamma_5 \partial_\mu \pi \psi + \frac{g_{\eta NN}}{2M_N} \bar{\psi} \gamma^\mu \gamma_5 \psi \partial_\mu \eta, \\
\mathcal{L}_\sigma &= g_{\sigma NN} \bar{\psi} \sigma \psi + \frac{e g_{\rho \gamma \sigma}}{2M_\rho} \text{Tr} [\tau^3 \partial_\mu \rho_\nu (\partial^\mu A^\nu - \partial^\nu A^\mu) \sigma], \\
\mathcal{L}_{\gamma NN} &= e \bar{\psi} \left(\gamma_\mu \frac{1 + \tau_3}{2} A^\mu - \frac{\kappa_N}{2M_N} \sigma^{\mu\nu} \partial_\nu A_\mu \right) \psi, \\
\mathcal{L}_{VNN} &= \frac{g_{\rho NN}}{2} \bar{\psi} \left(\gamma_\mu \rho^\mu - \frac{\kappa_\rho}{2M_N} \sigma^{\mu\nu} \partial_\nu \rho_\mu \right) \psi + g_{\omega NN} \bar{\psi} \left(\gamma_\mu \omega^\mu - \frac{\kappa_\omega}{2M_N} \sigma^{\mu\nu} \partial_\nu \omega_\mu \right) \psi, \quad (8)
\end{aligned}$$

where π ($= \boldsymbol{\tau} \cdot \boldsymbol{\pi}$), η , ρ_μ ($= \boldsymbol{\tau} \cdot \boldsymbol{\rho}_\mu$), and ω_μ are the pion, eta, rho, and omega meson fields, respectively. The photon field is represented by A_μ , and ψ and σ are the nucleon and σ meson fields, respectively. M_N (M_V) is the nucleon (vector meson) mass and κ_N is the anomalous magnetic moment of the nucleon, $\kappa_p = 1.79$ and $\kappa_n = -1.91$. Throughout this work we use the convention that $\varepsilon^{0123} = +1$.

The coupling constants of the Lagrangian (8) are determined as follows. First the coupling constants in $\mathcal{L}_{V\gamma\varphi}$ are determined by the vector meson radiative decay widths given by the Particle Data Group (PDG) [10]. In $\mathcal{L}_{VV\varphi}$, the coupling $g_{\omega\rho\pi}$ has been estimated by many models including the massive Yang-Mills approach [11], the hidden gauge approach [12], the vector meson dominance model [13], the unitary effective resonance model [14], and QCD sum rules [15]. All of these models predict that the value of $g_{\omega\rho\pi}$ is in the range of 10–16 GeV^{-1} . In this work we use $g_{\omega\rho\pi} = 12.9 \text{ GeV}^{-1}$ [16].

For $\mathcal{L}_{\varphi NN}$, we use the well-known value $g_{\pi NN}^2/4\pi = 14.0$ and $g_{\eta NN}^2/4\pi = 0.99$ determined [7, 17] by using the SU(3) relation. For σ meson, its mass and couplings to the nucleon and the vector mesons are highly model-dependent. Following Ref. [18], we set $M_\sigma = 0.5 \text{ GeV}$ and determine the coupling constants of the σ meson by reproducing the experimental data of ρ photoproduction at low energies, as explained in Refs. [18, 19]. Since the branching ratio of $\omega \rightarrow \pi\pi\gamma$ is very small [10], we do not consider the $\omega\gamma\sigma$ coupling in this model.

Following Refs. [7, 19], the values of the coupling constants $g_{\omega NN}$ and $g_{\rho NN}$ are taken from the analyses of πN scattering, pion photoproduction, and nucleon-nucleon scattering [8, 20]. All of the coupling constants used in our calculations are summarized in Table I.

In addition to the tree-diagrams which can be calculated by using the Lagrangian (8), we also include the Pomeron exchange in the amplitudes of vector meson photoproduction [21, 22, 23], although its contribution is relatively small at low energies. The details of the Pomeron exchange can be found, for example, in Refs. [7, 24], and will not be repeated here.

The considered tree-diagrams are then illustrated in Fig. 1 for $\gamma p \rightarrow \omega p$, Fig. 2 for $\pi N \rightarrow \omega p$, Fig. 3 for $\gamma p \rightarrow \rho^0 p$, and Fig. 4 for $\rho^0 p \rightarrow \omega p$. The calculations of these tree-diagrams are straightforward and therefore are not detailed here. These amplitudes are regularized by form factors as follows. For the t -channel exchanges, we use

$$F_t(t) = \frac{\Lambda^2 - M_{\text{ex}}^2}{\Lambda^2 - t} \quad (9)$$

for each vertex, where M_{ex} is the mass of the exchanged particle. For the s and u channel diagrams, we include [25]

$$F_{su}(r) = \frac{\Lambda_B^4}{\Lambda_B^4 - (r - M_B^2)^2}, \quad (10)$$

where $r = (s, u)$ and M_B is the mass of the intermediate baryon, i.e., the nucleon in our case. For the cutoff parameters in the tree-diagrams for $\gamma p \rightarrow \omega p$, we use the values adopted

in Ref. [7],

$$\Lambda_{\pi NN} = 0.6, \quad \Lambda_{\eta NN} = 1.0, \quad \Lambda_{\omega\pi\gamma} = 0.77, \quad \Lambda_{\omega\eta\gamma} = 0.9, \quad \Lambda_N = 0.5 \quad (11)$$

in GeV unit and the other cutoff parameters used for the other reactions will be specified later in Sec. IV. The gauge invariance of the nucleon pole terms are restored by making use of the projection operators as in Ref. [7].

The $\gamma N \rightarrow \pi N$ amplitudes are not discussed here because no tree-diagram model until now can describe the data in the considered energy region. Instead we construct the non-resonant amplitudes for $\gamma p \rightarrow \pi^0 p$ and $\gamma p \rightarrow \pi^+ n$ by subtracting the resonance amplitudes from the empirical multipole amplitudes of the SAID program [26]. The $\gamma N \rightarrow \pi N$ resonant amplitudes are calculated by using the procedure given in Ref. [27] except that we use the resonance parameters from PDG, not from those of Capstick and Roberts [28]. This shows that our non-resonant amplitudes for pion photoproduction are dependent on the models of nucleon resonances. Since the validity of the SAID program is limited up to $W \sim 2$ GeV, we restrict our consideration to ω photoproduction near threshold.

IV. RESULTS AND DISCUSSIONS

We can now perform the calculations based on Eqs. (1) – (3). The resonant term of Eq. (1) can be investigated, e.g., by using the quark models on nucleon resonances as in Refs. [6, 19]. Our focus in this work is therefore on the non-resonant term $t_{\gamma N, \omega N}$ defined by Eq. (2). The term $B_{\gamma N, \omega N}$ is calculated from the tree-diagrams illustrated in Fig. 1. The coupled-channel effects are included in the second term of Eq. (2), which is represented graphically in Fig. 5. Explicitly, this coupled-channel amplitude in the center of mass frame is obtained from performing the following loop-integration

$$t_{\gamma N, \omega N}(\mathbf{k}, \mathbf{q}; E) = \sum_{M=\pi, \rho} \int d\mathbf{q}' B_{\gamma N, MN}(\mathbf{k}, \mathbf{q}') \frac{1}{E - E_M(\mathbf{q}') - E_N(\mathbf{q}') + i\epsilon} t_{MN, \omega N}(\mathbf{q}', \mathbf{q}), \quad (12)$$

where \mathbf{k} and \mathbf{q} are the momentum for the photon and pion, respectively. The loop integral is regularized via the form factor in the form of $F_\ell(\mathbf{k})/F_\ell(\mathbf{k}_F)$, where

$$F_\ell = \left(\frac{\Lambda_\ell^2}{\Lambda_\ell^2 + \mathbf{k}^2} \right)^2 \quad (13)$$

and \mathbf{k} is the three-momentum of the intermediate particles in the center-of-mass frame while \mathbf{k}_F is their on-shell momentum. For the cutoff parameter, we use $\Lambda_\ell = 1$ GeV.

We first consider the coupled-channel effects due to the intermediate πN channel in Eq. (12). As discussed in the previous Section, the non-resonant $B_{\gamma N, \pi N}$ is generated by using the procedure of Ref. [27] to subtract the resonant amplitudes from the empirical $\gamma N \rightarrow \pi N$ amplitudes. Thus our results depend on the employed $\pi N \rightarrow \omega N$ amplitude. To proceed, we adjust the form factors of the tree-diagrams of Fig. 2 to fit the $\pi N \rightarrow \omega N$ data. In addition to the ρ and nucleon exchanges allowed by the Lagrangian (8), we also consider the exchange of the axial vector $b_1(1235)$ meson that was considered to explain the $\pi N \rightarrow \omega N$ reaction at high energies. However, we find that its contribution is negligibly small in the considered energy region. The details on the b_1 -exchange amplitude are summarized in Appendix. Our

numerical results show that the $\pi^- p \rightarrow \omega n$ data¹ near threshold can be described to some extent by choosing the following parameters

$$\Lambda_{\omega\rho\pi} = \Lambda_{\rho NN} = 1.55 \text{ GeV}, \quad \Lambda_{b_1\omega\pi} = \Lambda_{b_1NN} = 1.4 \text{ GeV}, \quad \Lambda_N = 0.5 \text{ GeV}. \quad (14)$$

The results are the solid lines in Figs. 6 and 7. In the same figure, we also show the results (dashed curves) calculated with

$$\Lambda_{\omega\rho\pi} = \Lambda_{\rho NN} = 1.3 \text{ GeV}. \quad (15)$$

The dashed curve in Fig. 7 is close to the results from the coupled-channel K -matrix model of Ref. [32] when the resonance contributions and the coupled-channel effects are neglected.² We thus interpret that the model corresponding to the dashed curves of Fig. 7 can be used to generate the non-resonant $\pi N \rightarrow \omega N$ amplitude for the calculation according to Eq. (2) or Eq. (12).

With the non-resonant amplitudes of $\gamma N \rightarrow \pi N$ and $\pi N \rightarrow \omega N$ transition obtained above, we now use Eq. (12) to compute the coupled-channel contributions due to the intermediate πN channel. As shown in Fig. 8, its magnitudes (dashed lines) are smaller than those of the tree-diagrams (dotted lines). However it can have significant effects through its interference with the tree-diagram amplitude. This is evident by comparing the results (solid curves) from the full calculation and the dotted curves. The coupled-channel effects are even more dramatic in determining the polarization observables. An example is shown in Fig. 9. We see that the coupled-channel effects can change the photon asymmetry in magnitudes at all angles.

We now turn to investigating the coupled-channel effects due to the ρN channel. From the very limited data [34, 38], we know that ρ^\pm photoproduction is much weaker than ρ^0 photoproduction. We therefore only keep $\rho^0 p$ in the loop integration (12). The $\gamma p \rightarrow \rho^0 p$ amplitude is generated from the tree diagrams in Fig. 3 and the $\rho^0 p \rightarrow \omega p$ amplitude from the tree diagrams in Fig. 4. We note that the tree-diagrams in Fig. 1 and Fig. 4 are related in the vector dominance model, except that the Pomeron and the η exchanges are not allowed in $\rho^0 p \rightarrow \omega p$ transition because of their quantum numbers.

We find that the constructed $\gamma p \rightarrow \rho^0 p$ amplitude (Fig. 3) can reproduce the total cross section data, if we use the following cutoff parameters (in unit of GeV) [19]

$$\Lambda_{\pi NN} = 0.6, \quad \Lambda_{\rho\pi\gamma} = 0.77, \quad \Lambda_{\sigma NN} = 1.0, \quad \Lambda_{\sigma\rho\gamma} = 0.9, \quad \Lambda_N = 0.5. \quad (16)$$

Our results are shown in Fig. 10. On the other hand, there is no data to constrain our model for $\rho^0 p \rightarrow \omega p$ (Fig. 4). Motivated by vector dominance model, therefore, we calculate these tree diagrams using the same form factors, given in Eq. (11), of Fig. 1 for ω photoproduction. The predicted total cross sections of $\rho^0 p \rightarrow \omega p$ reaction are shown in Fig. 11. We find that its magnitude at the peak is a factor of about 3 larger than that in Fig. 7 for the $\pi^- p \rightarrow \omega n$ reaction. This assumption may lead to an unrealistic estimation of the coupled-channel effects due to ρN channel. Another uncertainty in the calculation of Eq. (12) with ρN intermediate state is that the correct input to the loop integration (12) is the non-resonant amplitude, not the full amplitudes constructed above. But there is no experimental

¹ For the interpretation of the experimental data of Ref. [29], we follow Ref. [30]. See also Refs. [16, 31] for the other interpretation.

² We are grateful to G. Penner for communications on the results of Ref. [32].

information we can use here to extract the non-resonant part from the full amplitude. For these reasons, we perform the loop integration (12) using the constructed full amplitudes of both the $\gamma p \rightarrow \rho^0 p$ and $\rho^0 p \rightarrow \omega p$ transitions, but will explore whether the $\gamma p \rightarrow \omega p$ data can be best reproduced by scaling the calculated ρN loop contribution by a constant $f_{\rho N}$.

We first present results calculated from setting $f_{\rho N} = 1$. The calculated coupled-channel effects due to the ρN channel are shown in Fig. 12. Comparison with the results given in Fig. 8 shows that the effects of the ρN channel are as large as or even bigger than those of the intermediate πN channel. Thus the full calculation (solid lines) including both πN and ρN channels gives large corrections to the tree-diagram results (dotted lines). As discussed above, these results with $f_{\rho N} = 1$ may not be realistic and can only be considered as an upper bound.

We next explore whether the data can be best reproduced by varying $f_{\rho N}$. This is only for examining the model dependence of our investigation, not for explaining the data. An example of our results is shown in Fig. 13. We see that if the ρN loop contribution is scaled by $f_{\rho N} = 1/\sqrt{2}$, the results (solid curves) are closer to the SAPHIR data on ω photoproduction [1]. The corresponding coupled-channel effects on photon asymmetry are shown in Fig. 14. Again, we see that the polarization effects are sensitive to the coupled-channel effects. However the coupled-channel effects alone have a difficulty to explain the observed angular dependence of the single photon asymmetry [3], which would indicate the role of the nucleon resonances in ω photoproduction.

V. FUTURE DEVELOPMENTS

In this paper, we compute the coupled-channel effects in ω photoproduction with the intermediate πN and ρN channels for the non-resonant background reaction amplitudes. Its magnitudes are found to be comparable to those of the nucleon resonance contributions investigated in Ref. [7]. This indicates that such effects should be carefully taken into account when one extracts resonance parameters from the forthcoming experimental data.

Our calculation for the intermediate πN channel is rather well constrained by experimental information. However the ρN channel lacks such solid information and hence its contribution cannot be well estimated. Therefore our results for the ρN channel can be regarded as only an upper bound. For more concrete estimate on the ρN channel we need the non-resonant amplitudes of ρ photoproduction as well as the development of the models on $\rho N \rightarrow \omega N$ reaction although vector meson dominance can give us a guide to the latter reaction.

Among the possible intermediate states, we do not consider the ωN channel in the loop calculation. Inclusion of the ωN channel would be necessary to have the unitary amplitudes, but will lead to readjustment of the cutoff parameters in the tree-diagrams. Although naive speculation on the vector meson photoproduction data leads to that the intermediate ωN channel effects is suppressed by the ρN channel by a factor of 3, the ωN channel should be considered in the full calculation. Since the estimated coupled-channel effects are shown to be as large as those of the nucleon resonances, it would be crucial to test the models through other physical quantities such as spin asymmetries. For this purpose, we compute the single photon asymmetry and found that the coupled-channel effects are crucial at all scattering angles. But the difficulty of explaining the angle dependence of the asymmetries indicates the role of nucleon resonances in omega photoproduction at the resonance region. Improving the models for the non-resonant amplitudes as well as the full coupled-channel

calculations which will produce the unitary amplitudes are therefore strongly deserved to future study.

Acknowledgments

Y.O. is grateful to the Physics Division of Argonne National Laboratory for the hospitality. This work was supported in part by the Brain Korea 21 project of Korean Ministry of Education, the International Collaboration Program of KOSEF under Grant No. 20006-111-01-2, and U.S. DOE Nuclear Physics Division Contract No. W-31-109-ENG-38.

*

APPENDIX A: THE AXIAL $b_1(1235)$ MESON EXCHANGE IN $\pi N \rightarrow \omega N$

In this Appendix, we discuss the axial vector $b_1(1235)$ meson exchange in $\pi N \rightarrow \omega N$ reaction. Recently, this reaction has been studied by effective Lagrangian method and unitary coupled channel models focusing on the role of the nucleon resonances [16, 32, 39, 40, 41]. In the early investigations in 1960's and 1970's this reaction was studied in some detail mostly based on Regge theory and absorption models and at higher energies [42, 43, 44, 45, 46]. Based on the Regge theory, the b_1 trajectory exchange has been discussed as the secondary exchange process in $\pi N \rightarrow \omega N$ in addition to the major ρ -trajectory exchange. The main motivation for the secondary exchange was to account for the experimentally observed non-vanishing vector meson density matrix ρ_{00} that is expected to vanish if the natural-parity ρ -trajectory exchange dominates. The $b_1(1235)$ meson has quantum numbers $I^G(J^{PC}) = 1^+(1^{+-})$ with mass $M_{b_1} = 1230$ MeV and width $\Gamma_{b_1} = 142 \pm 9$ MeV, and it mostly decays into the $\omega\pi$ channel [10]. Thus its exchange can contribute to $\pi N \rightarrow \omega N$ as an unnatural parity exchange. In this work we consider the one- b_1 -exchange process (not the exchange of b_1 trajectory) in $\pi N \rightarrow \omega N$.

The general form of the $b_1\omega\pi$ interaction can be written as [47]

$$\mathcal{M}_{b_1\omega\pi} = -iM_{b_1}\varepsilon_\mu^*(\omega) \left[fg^{\mu\nu} + \frac{h}{M_\omega M_{b_1}} q^\nu k^\mu \right] \varepsilon_\nu(b_1), \quad (\text{A1})$$

where k and q are the momenta of the b_1 and ω , respectively, and $\varepsilon_\mu(b_1)$ and $\varepsilon_\mu(\omega)$ are their polarization vectors. Then the total decay width reads

$$\Gamma_{b_1 \rightarrow \omega\pi} = \frac{|\mathbf{q}|}{24\pi} \left\{ 2f^2 + \frac{1}{M_\omega^4} (E_\omega M_\omega f + |\mathbf{q}|^2 h)^2 \right\}, \quad (\text{A2})$$

where E_ω is the ω meson energy in the b_1 rest frame. The unknown coupling constants f and h can then be determined by the decay width and the D/S amplitude ratio in the decay of $b_1 \rightarrow \omega\pi$, where Eq. (A1) gives [48]

$$f^D/f^S = -\frac{\sqrt{2} \{ M_\omega (E_\omega - M_\omega) f + |\mathbf{q}|^2 h \}}{M_\omega (E_\omega + 2M_\omega) f + |\mathbf{q}|^2 h}, \quad (\text{A3})$$

which is defined from

$$\langle \omega(\mathbf{q}, m_\omega) \pi(-\mathbf{q}) | H_{\text{int}} | b_1(\mathbf{0}, m_b) \rangle = i f^S \delta_{m_\omega m_b} Y_{00}(\Omega_q) + i f^D \sum_{m_\ell} \langle 2 m_\ell 1 m_\omega | 1 m_b \rangle Y_{2m_\ell}(\Omega_q), \quad (\text{A4})$$

where $Y_{\ell m}(\Omega)$ and $\langle j_1 m_1 j_2 m_2 | j m \rangle$ are the spherical harmonics and Clebsch-Gordan coefficients, and m_ω (m_b) is the spin projection along the z axis for the ω (b_1) meson. Using the PDG [10] values for $\Gamma_{b_1 \rightarrow \omega\pi}$ and f^D/f^S , i.e., $\Gamma_{b_1 \rightarrow \omega\pi} = 142 \pm 9$ MeV and $f^D/f^S = 0.29 \pm 0.04$, we obtain

$$f \approx 3.71, \quad h \approx -11.38, \quad (\text{A5})$$

which gives $h/f \approx -3.1$. This should be compared with the value $h/f = +9.0$ used by Ref. [43] to fit the high energy data of $\pi N \rightarrow \omega N$ together with the ρ -trajectory exchange.

The b_1 -nucleon coupling can be written as

$$\mathcal{M}_{b_1 NN} = \frac{ig_{b_1 NN}}{2M_N} \bar{\psi} \sigma^{\mu\nu} \gamma_5 q^\nu \boldsymbol{\tau} \cdot \mathbf{b}_\mu \psi, \quad (\text{A6})$$

due to the G parity of the b_1 , where b_μ is the b_1 meson field and ψ is the nucleon. The momentum of the b_1 meson is denoted by q_μ . The coupling constant $g_{b_1 NN}$ is related to the nucleon tensor charge and has been recently estimated by making use of the axial vector dominance and $SU(6) \times O(3)$ spin-flavor symmetry in Ref. [49] in a similar way to Ref. [50]. (See also Ref. [51].) The result reads

$$g_{b_1 NN} = \frac{5}{3\sqrt{2}} g_{a_1 NN}. \quad (\text{A7})$$

Using $g_{a_1 NN} \approx 7.49$, one finally obtains $g_{b_1 NN} \approx 8.83$ [49].

Thus the production amplitude for the reaction of $\pi N \rightarrow \omega N$ is obtained as

$$\begin{aligned} \mathcal{M} = & \frac{M_{b_1} g_{b_1 NN} C_I}{2M_N [(k-q)^2 - M_{b_1}^2]} \varepsilon_\mu^*(\omega) \left\{ f g^{\mu\nu} + \frac{h}{M_\omega M_{b_1}} q^\nu (k-q)^\mu \right\} \\ & \times \left\{ g_{\nu\alpha} - \frac{(k-q)_\nu (k-q)_\alpha}{M_{b_1}^2} \right\} \bar{u}(p') \gamma_5 \sigma^{\alpha\beta} (k-q)_\beta u(p), \end{aligned} \quad (\text{A8})$$

where $u(p)$ is the Dirac spinor of the nucleon with momentum p . The isospin factor C_I is

$$C_I = \begin{cases} \sqrt{2} & \text{for } \pi^- p \rightarrow \omega n, \pi^+ n \rightarrow \omega p \\ +1 & \text{for } \pi^0 p \rightarrow \omega p \\ -1 & \text{for } \pi^0 n \rightarrow \omega n \end{cases} \quad (\text{A9})$$

Given in Fig. 15 are the total cross sections for $\pi^- p \rightarrow \omega n$. The solid and dashed lines are obtained with the ρ exchange and the nucleon pole terms with the cutoff parameters (14) and (15), respectively. The total cross section due to the b_1 exchange is given by the dot-dashed line. For the form factor, we use the form of Eq. (9) with $\Lambda_{b_1 \omega\pi} = \Lambda_{b_1 NN} = 1.4$ GeV. Since its contribution is suppressed by ρ and nucleon exchange contributions, the b_1 exchange is magnified in Fig. 15 by a factor of 50. This conclusion does not sensitively depend on the cutoff parameters $\Lambda_{b_1 \omega\pi}$ and $\Lambda_{b_1 NN}$, when they are larger than the exchanged meson mass M_{b_1} .

[1] F. J. Klein, Ph.D. thesis, Bonn University (1996); πN Newslett. **14**, 141 (1998).

[2] CLAS Collaboration, E. Anciant *et al.*, Phys. Rev. Lett. **85**, 4682 (2000); CLAS Collaboration, K. Lukashin *et al.*, Phys. Rev. C **63**, 065205 (2001); CLAS Collaboration, M. Battaglieri *et al.*, Phys. Rev. Lett. **87**, 172002 (2001).

[3] J. Ajaka *et al.*, in Proceedings of 14th International Spin Physics Symposium (SPIN 2000), Oct. 2000, Edited by K. Hatanaka, T. Nakano, K. Imai, and H. Ejiri, AIP Conf. Proc. **570**, 198 (2001).

[4] LEPS Collaboration, T. Nakano, in Proceedings of 14th International Spin Physics Symposium (SPIN 2000), Oct. 2000, Edited by K. Hatanaka, T. Nakano, K. Imai, and H. Ejiri, AIP Conf. Proc. **570**, 189 (2001).

[5] S. Capstick and W. Roberts, Prog. Part. Nucl. Phys. **45**, S241 (2000), and references therein.

[6] Q. Zhao, Z. Li, and C. Bennhold, Phys. Rev. C **58**, 2393 (1998); Q. Zhao, *ibid.* **63**, 025203 (2001).

[7] Y. Oh, A. I. Titov, and T.-S. H. Lee, Phys. Rev. C **63**, 025201 (2001).

[8] T. Sato and T.-S. H. Lee, Phys. Rev. C **54**, 2660 (1996).

[9] K. Schilling and F. Storim, Nucl. Phys. **B7**, 559 (1968).

[10] Particle Data Group, D. E. Groom *et al.*, Eur. Phys. J. C **15**, 1 (2000).

[11] Ö. Kaymakcalan, S. Rajeev, and J. Schechter, Phys. Rev. D **30**, 594 (1984); P. Jain, R. Johnson, U.-G. Meissner, N. W. Park, and J. Schechter, *ibid.* **37**, 3252 (1988).

[12] T. Fujiwara, T. Kugo, H. Terao, S. Uehara, and K. Yamawaki, Prog. Theor. Phys. **73**, 926 (1985).

[13] F. Klingl, N. Kaiser, and W. Weise, Z. Phys. A **356**, 193 (1996).

[14] F. Kleefeld, E. van Beveren, and G. Rupp, Nucl. Phys. **A694**, 470 (2001).

[15] V. L. Eletsky, B. L. Ioffe, and Y. I. Kogan, Phys. Lett. **122B**, 423 (1983).

[16] A. I. Titov, B. Kämpfer, and B. L. Reznik, FZ Rossendorf Report (2001), nucl-th/0102032.

[17] A. Titov, T.-S. H. Lee, H. Toki, and O. Streltsova, Phys. Rev. C **60**, 035205 (1999).

[18] B. Friman and M. Soyeur, Nucl. Phys. **A600**, 477 (1996).

[19] Y. Oh, A. I. Titov, and T.-S. H. Lee, talk at NSTAR2000 Workshop, Jefferson Lab., Feb. 2000 (2000), nucl-th/0004055.

[20] Th. A. Rijken, V. G. J. Stoks, and Y. Yamamoto, Phys. Rev. C **59**, 21 (1999).

[21] A. Donnachie and P. V. Landshoff, Nucl. Phys. **B244**, 322 (1984); Phys. Lett. B **296**, 227 (1992).

[22] J.-M. Laget and R. Mendez-Galain, Nucl. Phys. **A581**, 397 (1995).

[23] M. A. Pichowsky and T.-S. H. Lee, Phys. Rev. D **56**, 1644 (1997).

[24] A. I. Titov, Y. Oh, S. N. Yang, and T. Morii, Phys. Rev. C **58**, 2429 (1998).

[25] B. C. Pearce and B. K. Jennings, Nucl. Phys. **A528**, 655 (1991).

[26] Partial-Wave Analysis Facility (SAID), R. A. Arndt, W. J. Briscoe, R. L. Workman, and I. I. Strakovsky, <http://gwdac.phys.gwu.edu>.

[27] D. Dutta, H. Gao, and T.-S. H. Lee, Phys. Rev. C **65**, 044619 (2002).

[28] S. Capstick, Phys. Rev. D **46**, 2864 (1992); S. Capstick and W. Roberts, *ibid.* **49**, 4570 (1994).

[29] H. Karami, J. Carr, N. C. Debenham, D. A. Garbutt, W. G. Jones, D. M. Binnie, J. Keyne, P. Moissidis, H. N. Sarma, and I. Siotis, Nucl. Phys. **B154**, 503 (1979).

[30] G. Penner and U. Mosel, Universität Giessen Report (2001), nucl-th/0111024.

- [31] C. Hanhart and A. Kudryavtsev, Eur. Phys. J. A **6**, 325 (1999).
- [32] G. Penner and U. Mosel, Universität Giessen Report (2001), nucl-th/0111023.
- [33] J. S. Danburg, M. A. Abolins, O. I. Dahl, D. W. Davies, P. L. Hoch, J. Kirz, D. H. Miller, and R. K. Rader, Phys. Rev. D **2**, 2564 (1970); J. Keyne, D. M. Binnie, J. Carr, N. C. Debenham, A. Duane, D. A. Garbutt, W. G. Jones, I. Siotis, and J. G. McEwen, *ibid.* **14**, 28 (1976).
- [34] Aachen-Hamburg-Heidelberg-München Collaboration, W. Struczinski *et al.*, Nucl. Phys. **B108**, 45 (1976).
- [35] W. Struczinski *et al.*, Nucl. Phys. **B47**, 436 (1972).
- [36] ABBHHM Collaboration, R. Erbe *et al.*, Phys. Rev. **175**, 1669 (1968).
- [37] J. Ballam, G. B. Chadwick, Z. G. T. Guiragossian, A. Levy, M. Menke, P. Seyboth, and G. E. Wolf, Phys. Lett. **30B**, 421 (1969); J. Ballam *et al.*, Phys. Rev. D **5**, 545 (1972); **7**, 3150 (1973).
- [38] D. P. Barber *et al.*, Z. Phys. C **2**, 1 (1979).
- [39] M. Lutz, G. Wolf, and B. Friman, Nucl. Phys. **A661**, 526c (1999).
- [40] M. F. M. Lutz, Gy. Wolf, and B. Friman, GSI Report No. GSI-01-30 (2001), nucl-th/0112052.
- [41] M. Post and U. Mosel, Nucl. Phys. **A688**, 808 (2001).
- [42] J. D. Jackson, J. T. Donohue, K. Gottfried, R. Keyser, and B. E. V. Svensson, Phys. Rev. **139**, B428 (1965).
- [43] M. Barmawi, Phys. Rev. **142**, 1088 (1966); Phys. Rev. Lett. **16**, 595 (1966); Phys. Rev. **166**, 1857 (1968).
- [44] F. Henyey, K. Kajantie, and G. L. Kane, Phys. Rev. Lett. **21**, 1782 (1968).
- [45] G. E. Hite and E. G. Krubasik, Nucl. Phys. **B29**, 465 (1971).
- [46] A. C. Irving and C. Michael, Nucl. Phys. **B82**, 282 (1974).
- [47] S. M. Berman and S. D. Drell, Phys. Rev. Lett. **11**, 220 (1963), (E) **11**, 303 (1963).
- [48] N. Isgur, C. Morningstar, and C. Reader, Phys. Rev. D **39**, 1357 (1989).
- [49] L. Gamberg and G. R. Goldstein, Phys. Rev. Lett. **87**, 242001 (2001).
- [50] M. Birkel and H. Fritzsch, Phys. Rev. D **53**, 6195 (1996).
- [51] N. I. Kochelev, D.-P. Min, Y. Oh, V. Vento, and A. V. Vinnikov, Phys. Rev. D **61**, 094008 (2000).

FIGURES

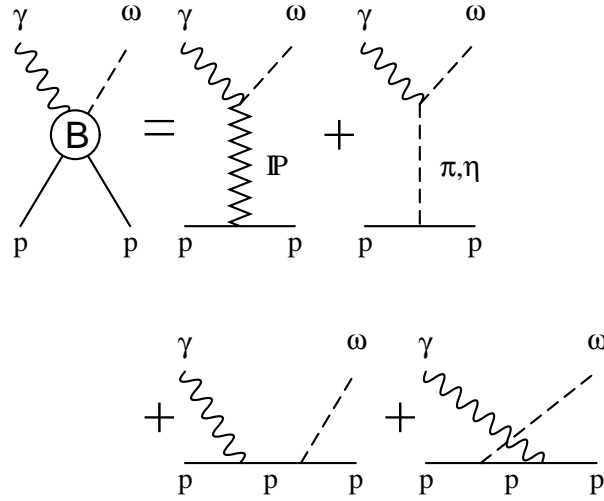


FIG. 1: Tree-diagrams for $\gamma p \rightarrow \omega p$ which include Pomeron exchange, π and η exchange, and the direct and crossed nucleon terms.

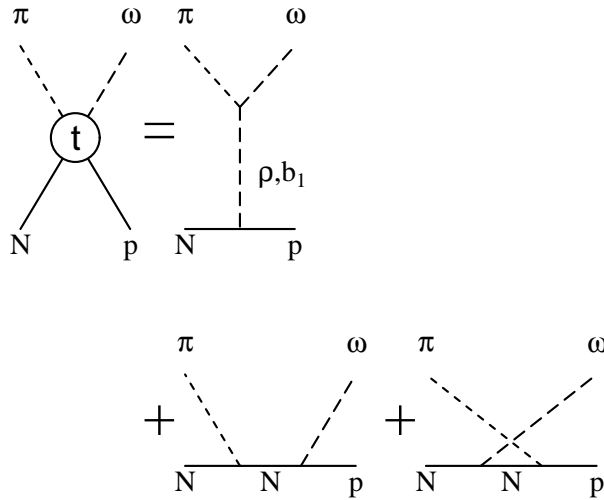


FIG. 2: Tree-diagrams for $\pi N \rightarrow \omega N$ which include ρ and b_1 exchanges and the nucleon pole terms.

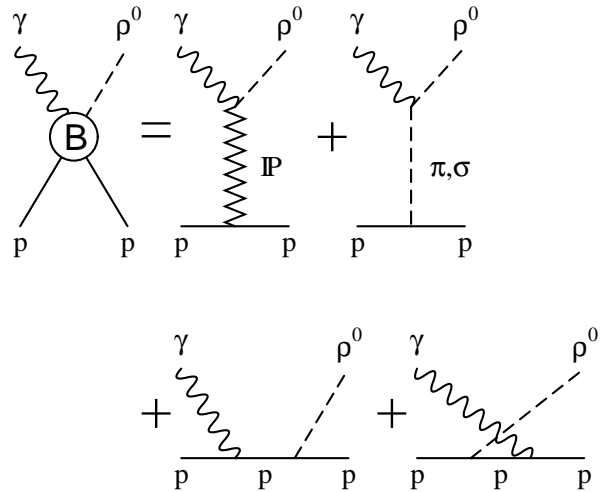


FIG. 3: Tree-diagrams for $\gamma p \rightarrow \rho p$ which include Pomeron, π , and σ meson exchanges and the nucleon pole terms.

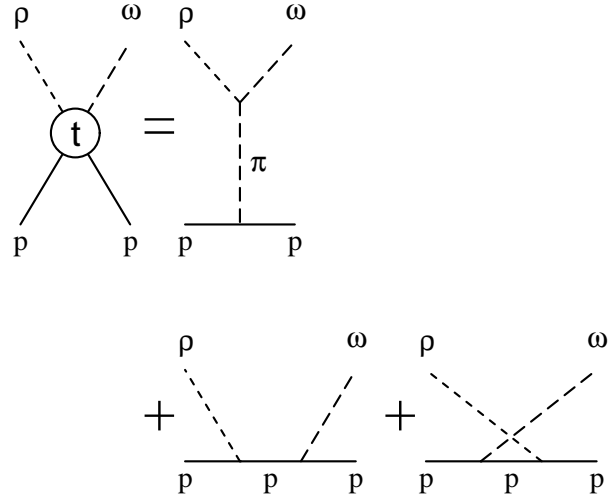


FIG. 4: Tree-diagrams for $\rho p \rightarrow \omega p$ which include one-pion exchange and the nucleon pole terms.

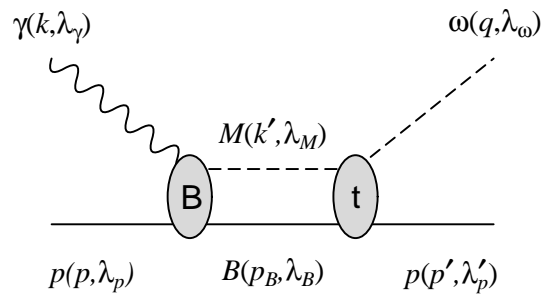


FIG. 5: Diagrammatic representation of the intermediate meson-baryon (MB) state in ω photoproduction.

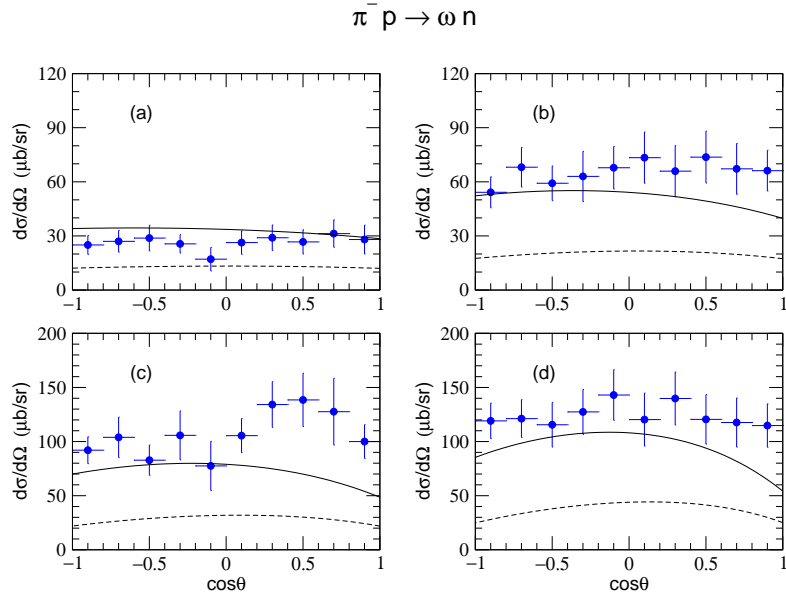


FIG. 6: Differential cross section for $\pi^- p \rightarrow \omega n$ at W = (a) 1.726 GeV, (b) 1.734 GeV, (c) 1.746 GeV, and (d) 1.762 GeV. The solid lines are obtained with $\Lambda_{\omega\rho\pi} = \Lambda_{\rho NN} = 1.55$ GeV and the dashed lines with $\Lambda_{\omega\rho\pi} = \Lambda_{\rho NN} = 1.3$ GeV. The experimental data are from Ref. [29].

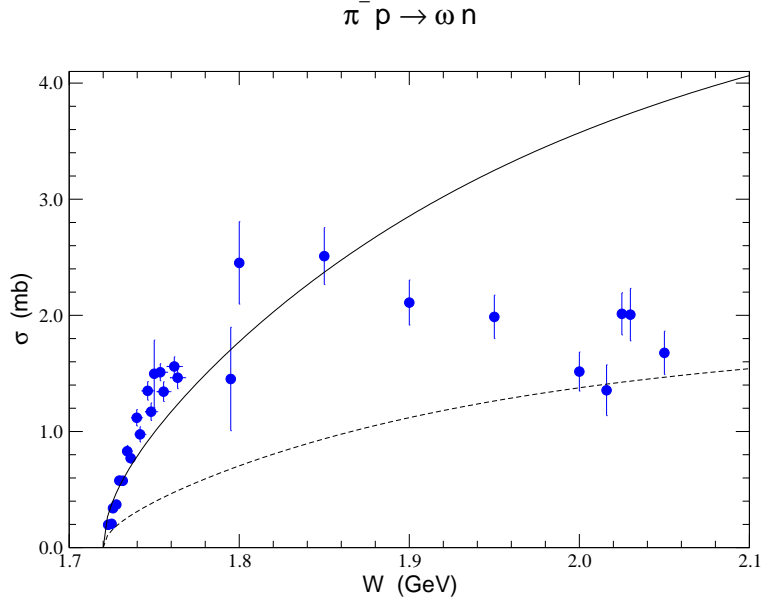


FIG. 7: Total cross section for $\pi^- p \rightarrow \omega n$. Notations are the same as in Fig. 6. The experimental data are from Refs. [29, 33].

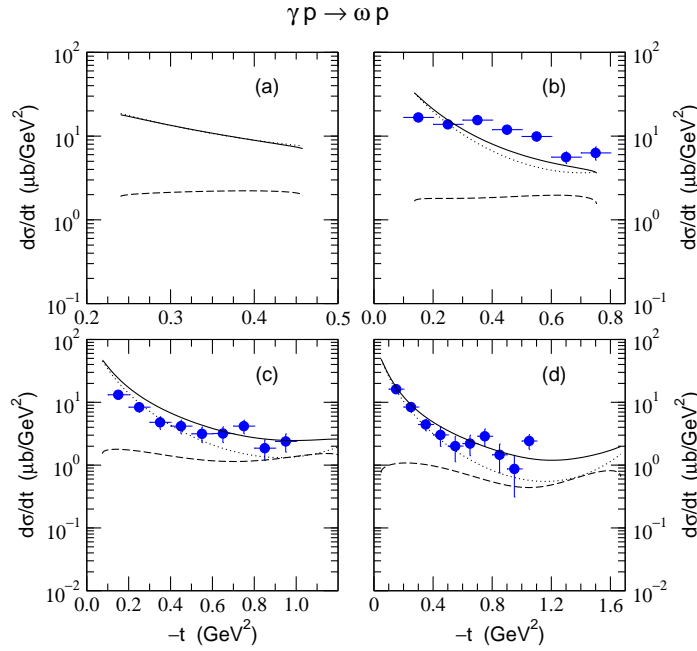


FIG. 8: Differential cross section for $\gamma p \rightarrow \omega p$ at E_γ = (a) 1.125 GeV, (b) 1.23 GeV, (c) 1.45 GeV, and (d) 1.68 GeV. The dotted lines are obtained from the tree diagrams and the dashed lines are from the intermediate πN channel. The solid lines are the full calculations. The experimental data are from SAPHIR [1].

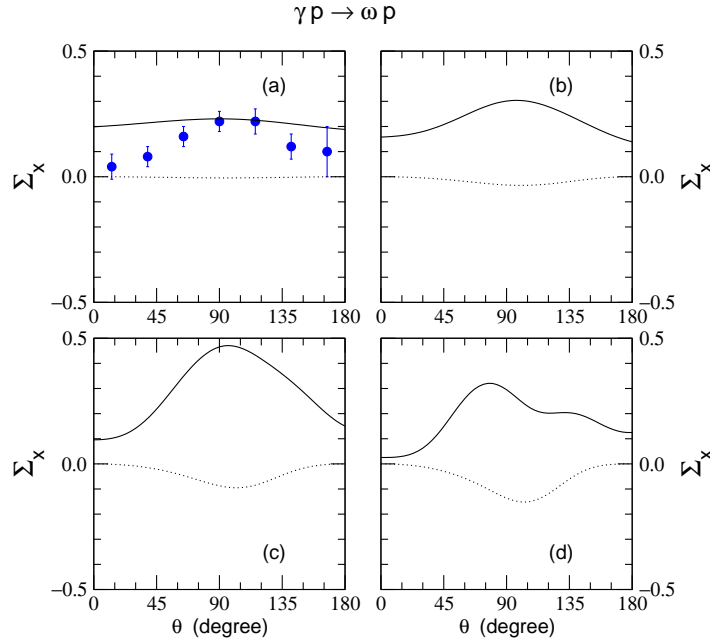


FIG. 9: Single photon asymmetry Σ_x for $\gamma p \rightarrow \omega p$ at $E_\gamma =$ (a) 1.125 GeV, (b) 1.23 GeV, (c) 1.45 GeV, and (d) 1.68 GeV. The dotted lines are from the backgrounds only while the solid lines include the intermediate πN channel. The experimental data are from Ref. [3]

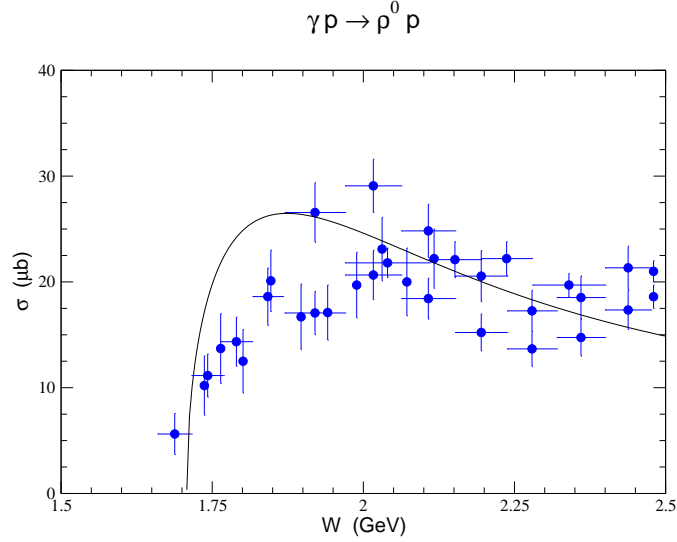


FIG. 10: Total cross section for $\gamma p \rightarrow \rho^0 p$. The solid line is obtained with the diagrams of Fig. 3. The experimental data are from Refs. [1, 34, 35, 36, 37].

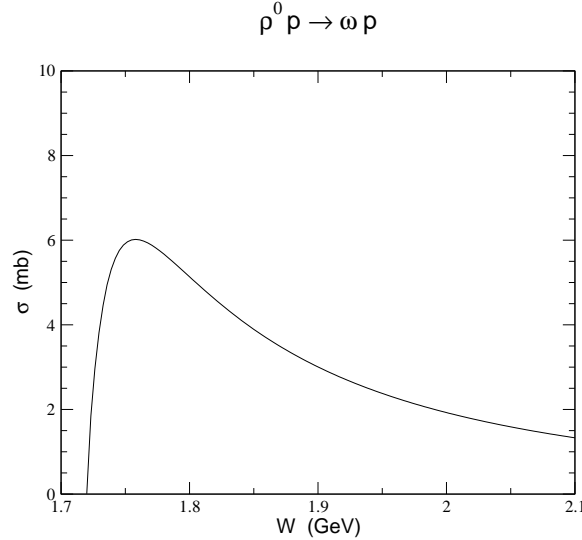


FIG. 11: Total cross section for $\rho^0 p \rightarrow \omega p$. The solid line is the result of the diagrams shown in Fig. 4.

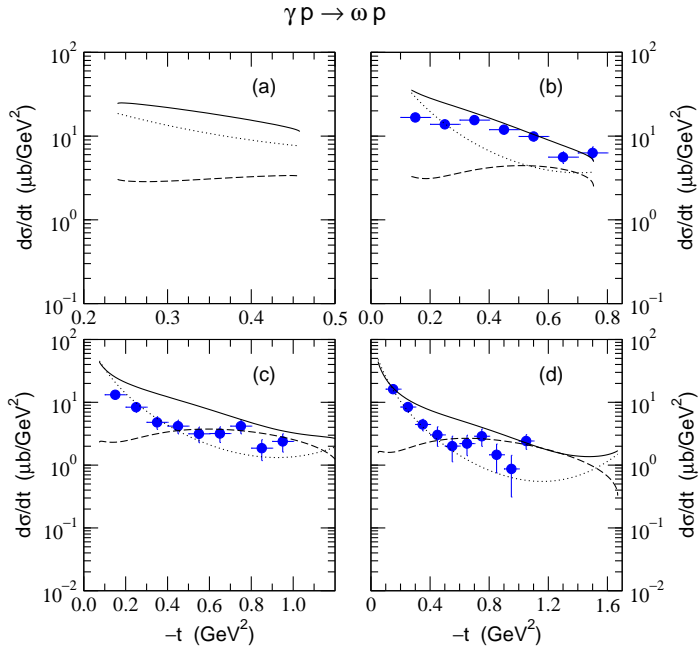


FIG. 12: Differential cross section for $\gamma p \rightarrow \omega p$ at E_γ = (a) 1.125 GeV, (b) 1.23 GeV, (c) 1.45 GeV, and (d) 1.68 GeV. The dotted lines are from the tree diagrams and the dashed lines from the intermediate ρN channel. The solid lines are the results of the full calculations including the tree diagrams and the intermediate πN and ρN channels. The experimental data are from SAPHIR [1].

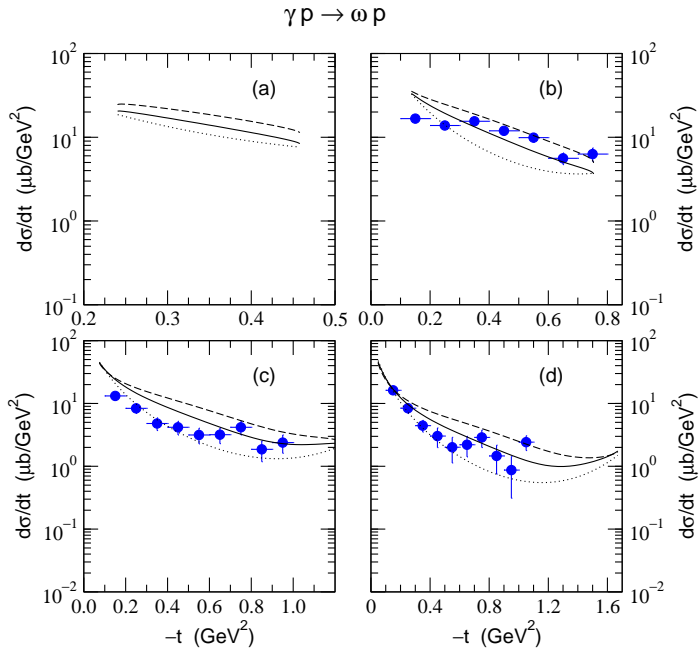


FIG. 13: Differential cross section for $\gamma p \rightarrow \omega p$ at E_γ = (a) 1.125 GeV, (b) 1.23 GeV, (c) 1.45 GeV, and (d) 1.68 GeV. The dotted lines are from the tree diagrams. The dashed lines are the results of the full calculations including the tree diagrams and the intermediate πN and ρN channels while the solid lines are the full results with $f_{\rho N} = 1/\sqrt{2}$. The experimental data are from SAPHIR [1].

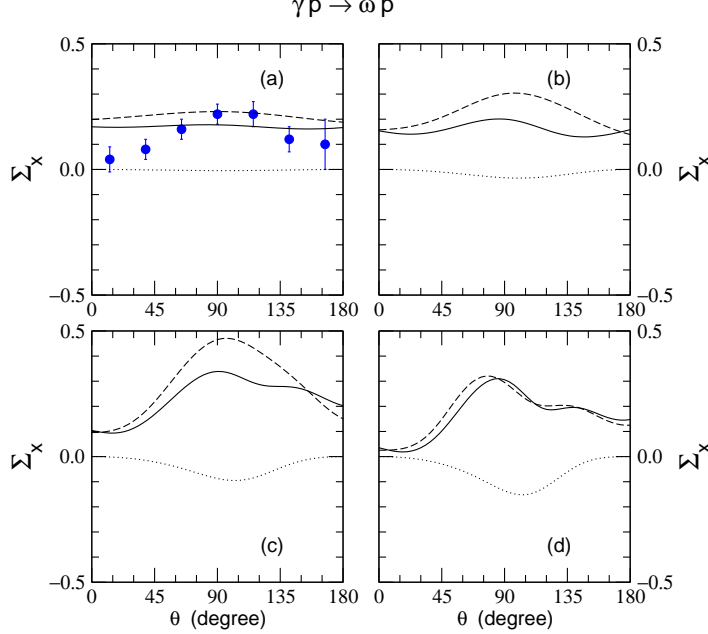


FIG. 14: Single photon asymmetry Σ_x for $\gamma p \rightarrow \omega p$ at E_γ = (a) 1.125 GeV, (b) 1.23 GeV, (c) 1.45 GeV, and (d) 1.68 GeV. The dotted lines are from the backgrounds only and the dashed lines include the intermediate πN channel. The full calculation with $f_{\rho N} = 1/\sqrt{2}$ are given by the solid lines. The experimental data are from Ref. [3]

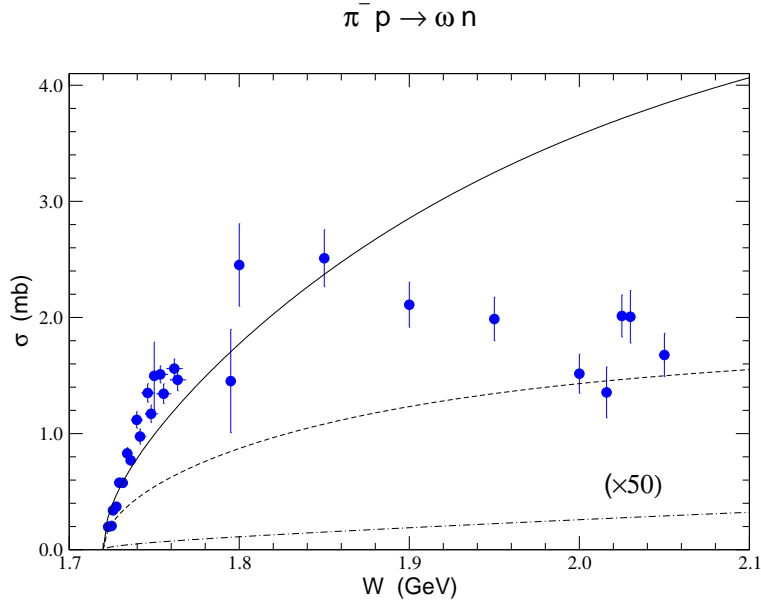


FIG. 15: Total cross section for $\pi^- p \rightarrow \omega n$. Solid and dashed lines are the same as in Fig. 6 while the dot-dashed line is from the $b_1(1235)$ exchange process (multiplied by 50). The experimental data are from Refs. [29, 33].

TABLES

TABLE I: Coupling constants of the effective Lagrangian (7).

coupling	value	coupling	value	coupling	value
$g_{\rho\gamma\pi}$	0.70	$g_{\pi NN}$	13.26	$g_{\rho NN}$	6.12
$g_{\omega\gamma\pi}$	1.82	$g_{\eta NN}$	3.53	κ_ρ	3.1
$g_{\omega\gamma\eta}$	0.42	$g_{\sigma NN}$	10.03	$g_{\omega NN}$	10.35
$g_{\omega\rho\pi}$	12.9 ^a	$g_{\rho\gamma\sigma}$	3.0	κ_ω	0.0

^ain GeV^{-1} unit